

Structural Studies of Yeast Δ^1 -Pyrroline-5-carboxylate Dehydrogenase (ALDH4A1): Active Site Flexibility and Oligomeric State

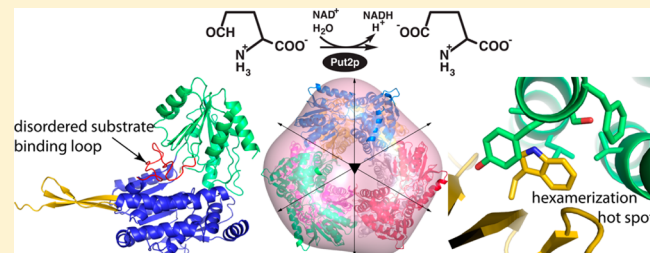
Travis A. Pemberton,[†] Dhiraj Srivastava,[†] Nikhilesh Sanyal,[‡] Michael T. Henzl,[§] Donald F. Becker,[‡] and John J. Tanner*,^{†,§}

[†]Department of Chemistry, University of Missouri—Columbia, Columbia, Missouri 65211, United States

[‡]Department of Biochemistry, University of Nebraska—Lincoln, Lincoln, Nebraska 68588, United States

[§]Department of Biochemistry, University of Missouri—Columbia, Columbia, Missouri 65211, United States

ABSTRACT: The proline catabolic enzyme Δ^1 -pyrroline-5-carboxylate dehydrogenase (ALDH4A1) catalyzes the NAD⁺-dependent oxidation of γ -glutamate semialdehyde to L-glutamate. In *Saccharomyces cerevisiae*, ALDH4A1 is encoded by the *PUT2* gene and known as Put2p. Here we report the steady-state kinetic parameters of the purified recombinant enzyme, two crystal structures of Put2p, and the determination of the oligomeric state and quaternary structure from small-angle X-ray scattering and sedimentation velocity. Using Δ^1 -pyrroline-5-carboxylate as the substrate, catalytic parameters k_{cat} and K_m were determined to be 1.5 s⁻¹ and 104 μM , respectively, with a catalytic efficiency of 14000 M⁻¹ s⁻¹. Although Put2p exhibits the expected aldehyde dehydrogenase superfamily fold, a large portion of the active site is disordered in the crystal structure. Electron density for the 23-residue aldehyde substrate-binding loop is absent, implying substantial conformational flexibility in solution. We furthermore report a new crystal form of human ALDH4A1 (42% identical to Put2p) that also shows disorder in this loop. The crystal structures provide evidence of multiple active site conformations in the substrate-free form of the enzyme, which is consistent with a conformational selection mechanism of substrate binding. We also show that Put2p forms a trimer-of-dimers hexamer in solution. This result is unexpected because human ALDH4A1 is dimeric, whereas some bacterial ALDH4A1s are hexameric. Thus, global sequence identity and domain of life are poor predictors of the oligomeric states of ALDH4A1. Mutation of a single Trp residue that forms knob-in-hole interactions across the dimer–dimer interface abrogates hexamer formation, suggesting that this residue is the center of a protein–protein association hot spot.



The mitochondrial enzymes Put1p and Put2p catalyze proline catabolism in *Saccharomyces cerevisiae* (Figure 1). Put1p is a flavin-dependent dehydrogenase that catalyzes the oxidation of L-proline to Δ^1 -pyrroline-5-carboxylate (PSC) and couples proline oxidation to reduction of ubiquinone.¹ Put2p is a PSC dehydrogenase (PSCDH, EC 1.2.1.88, formerly EC 1.5.1.12) and is also known as ALDH4A1 in reference to its membership in family 4 of the aldehyde dehydrogenase (ALDH) superfamily.² Put2p catalyzes the NAD⁺-dependent oxidation of γ -glutamate semialdehyde (GSA, the hydrolysis product of PSC) to L-glutamate. In total, the proline catabolic pathway catalyzes a four-electron oxidation of proline.

Several studies have shown that proline is important in various organisms for stress protection.³ The accumulation of proline in yeast leads to improved freeze tolerance.⁴ In contrast to that of proline, the accumulation of PSC is associated with toxicity effects and induced cell death in yeast.^{5,6} Coordinated expression of *PUT1* and *PUT2* is important for avoiding buildup of PSC. The *PUT1* and *PUT2* genes are upregulated by proline under nitrogen limiting conditions and, together with glutamate dehydrogenase, allow yeast to utilize proline as a

nitrogen source.⁷ The mechanism of PSC toxicity involves inhibition of mitochondrial respiration and an increased level of production of reactive oxygen species.⁵ Interestingly, an N-acetyltransferase enzyme known as Mpr1 acetylates PSC, thereby decreasing its level of accumulation and weakening its harmful effects in yeast.⁸

Mammalian PSCDHs have been characterized biochemically. Early studies of the human (HsPSCDH) and rat enzymes established the order of substrate binding and product release, as well as substrate preferences.^{9–11} More recent work on HsPSCDH and mouse PSCDH (MmPSCDH) provided additional details about the kinetic mechanism and the molecular basis of type II hyperprolinemia,¹² a metabolic disorder caused by a defect in ALDH4A1 function.^{13–15}

The three-dimensional structures of PSCDHs have been studied intensely. Tahirov's group reported the first PSCDH structure using the enzyme from *Thermus thermophilus*

Received: January 12, 2014

Revised: February 5, 2014

Published: February 6, 2014

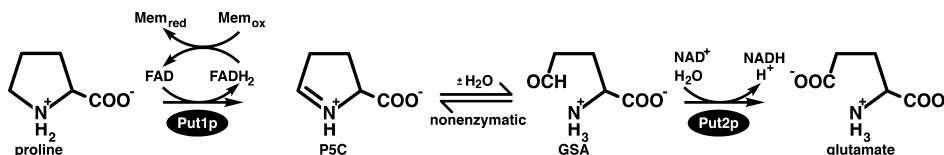


Figure 1. Reactions catalyzed by the yeast proline catabolic enzymes Put1p and Put2p.

(TtPSCDH).^{16,17} We subsequently determined the structures of HsPSCDH and MmPSCDH,^{12,18} and the New York Structural Genomics Research Consortium has deposited structures of two *Bacillus* PSCDHs in the Protein Data Bank (PDB) (entries 3QAN and 3RJL). Collectively, the structures confirmed PSCDH as a member of the ALDH superfamily, contributed additional information about the catalytic mechanism, and provided insight into the structural basis of cofactor and semialdehyde selectivity. We also determined the solution oligomeric states and quaternary structures of several PSCDHs.¹⁹ The human, mouse, and *Bacillus* enzymes are dimeric in solution, whereas TtPSCDH and *Deinococcus radiodurans* PSCDH (DrPSCDH) form trimer-of-dimers hexamers in solution. Thus, the protein fold, but not the oligomeric state, is conserved within the ALDH4A1 subfamily.

Although the yeast *PUT* genes were identified more than 30 years ago, the Put1p and Put2p enzymes have remained relatively understudied. Wanduragala et al. reported the purification and characterization of Put1p in 2010,¹ but analogous studies of Put2p have not appeared in the literature. We therefore have created a recombinant bacterial expression system for Put2p, measured the steady-state kinetic parameters of the purified enzyme, determined the crystal structure, and deduced the oligomeric state and quaternary structure in solution from small-angle X-ray scattering (SAXS).

EXPERIMENTAL PROCEDURES

Subcloning and Mutagenesis. The *PUT2* gene was obtained from M. Brandriss of the Rutgers New Jersey Medical School and subcloned into vectors pET14b using NdeI and XhoI and pKA8H between NdeI and BamHI restriction sites, resulting in pET14b-PUT2 and pKA8H-PUT2 constructs. DNA encoding residues 23–575, which lacks the N-terminal mitochondrial targeting peptide,²⁰ was amplified from pKA8H using AAACATATGAAGCCCCCAAGCACATAAG as the forward primer and the T7 terminator as the reverse primer. The resulting fragment was subcloned into pKA8H using NdeI and BamHI to give the pKA8H-PUT2Δ22 construct. The expressed protein has an N-terminal His₈ tag and tobacco etch virus protease cleavage site.

The W193A mutant of Put2p was created from pKA8H-PUT2Δ22 with the QuikChange II site-directed mutagenesis kit (Agilent) using the forward primer (5'-GGTACAATCTA-CCGTTGCTGACAGATCTGC-3') and reverse primer (5'-GCAGATCTGTAGCAAACGGTAGATTGTACC-3'). The mutation was confirmed using DNA sequencing.

Expression and Purification of Put2p. Put2p and Put2p mutant W193A were expressed in Bl21(DE3)pLysS cells. Cells were grown at 37 °C and 250 rpm until the OD₆₀₀ reached 0.6 and induced with 0.5 mM IPTG for 8 h at 22 °C and 200 rpm. The cells were harvested by centrifugation at 3500 rpm for 30 min and resuspended in 20 mM HEPES, 60 mM NaCl, and 5% glycerol (pH 8.0). Cells were quick frozen in liquid nitrogen and stored at –80 °C until they were further purified.

Thawed cells were broken by sonication and centrifuged at 16500 rpm for 1 h. The supernatant was applied to a HisTrap HP column that had been charged with Ni²⁺ and equilibrated with 20 mM HEPES, 300 mM NaCl, and 5% glycerol (pH 8.0). The column was washed with equilibration buffer supplemented with 30 mM imidazole, and the enzyme was eluted with 300 mM imidazole. Fractions containing Put2p were pooled, dialyzed into 50 mM Tris, 0.5 mM EDTA, 0.5 mM tris(hydroxymethyl)phosphine (THP), and 5% glycerol (pH 8.0), and loaded onto a HiTrap Q anion exchange column. Put2p was eluted with a linear gradient of NaCl from 0 to 1 M. Fractions were analyzed via sodium dodecyl sulfate–polyacrylamide gel electrophoresis, pooled, and dialyzed into 50 mM Tris, 150 mM NaCl, 0.5 mM EDTA, 0.5 mM THP, and 5% glycerol (pH 8.0).

Crystallization of Put2p. Crystallization trials were performed in sitting drops at 20 °C using drops formed by mixing 1 μL each of the enzyme and reservoir solutions. Crystal screening using commercially available kits (Hampton Research) was used to identify promising crystallization conditions.

Put2p expressed from pKA8H-PUT2Δ22, including the N-terminal His tag, was used for crystallization. Optimized crystals were grown using 8 mg/mL enzyme and a reservoir containing 8–14% (w/v) polyethylene glycol (PEG) 3350, 0.1 M (NH₄)₂SO₄, and 0.1 M Bis-Tris (pH 5.5–6.5). The crystals were cryoprotected with 15% PEG 3350, 0.1 M (NH₄)₂SO₄, 0.1 M Bis-Tris (pH 6.0), and 20% glycerol. The cryoprotected crystals were harvested with nylon loops (Hampton Research) and plunged into liquid nitrogen. The space group is *P*6₃ with *a* = 109 Å and *c* = 181 Å. The asymmetric unit contains one dimer and 51% solvent, based on the method of Matthews.²¹

Crystals of Put2p complexed with NAD⁺ were obtained by cocrystallization using the procedure described above for the ligand-free crystals. A stock solution containing 10 mM NAD⁺ and 7 mg/mL enzyme was used for crystallization. Optimized crystals were grown by combining this stock and an equal volume of a reservoir containing 8–14% (w/v) PEG 3350, 0.1 M (NH₄)₂SO₄, and 0.1 M Bis-Tris (pH 5.5–6.5). These crystals were cryoprotected with 12% PEG 3350, 0.1 M (NH₄)₂SO₄, 10 mM NAD⁺, 0.1 M Bis-Tris (pH 5.5), and 15% (v/v) PEG 200. The cryoprotected crystals were harvested with nylon loops and plunged into liquid nitrogen. The space group is *P*6₃ with *a* = 108 Å and *c* = 181 Å with a dimer in the asymmetric unit.

Expression, Purification, and Crystallization of Tag-Free HsPSCDH. HsPSCDH residues 18–563 with an N-terminal His tag were expressed and purified as described previously.¹² The His tag was removed with thrombin as follows. The purified protein was dialyzed into thrombin cleavage buffer [20 mM Tris, 150 mM NaCl, 2.5 mM CaCl₂, and 5% glycerol (pH 8.0)] and incubated with thrombin (1 unit of thrombin per 4 mg of HsPSCDH) for 1 day at 4 °C. Thrombin was removed using a HiTrap Benzamidine FF affinity column. The cleaved His tag and residual unprocessed

Table 1. X-ray Diffraction Data Collection and Refinement^a

	Put2p	Put2p–NAD ⁺	HsPSCDH
space group	$P6_3$	$P6_3$	$P2_1$
unit cell dimensions	$a = 109.0 \text{ \AA}, c = 181.2 \text{ \AA}$	$a = 108.0 \text{ \AA}, c = 181.0 \text{ \AA}$	$a = 92.0 \text{ \AA}, b = 121.3 \text{ \AA}, c = 93.4 \text{ \AA}, \beta = 104.2^\circ$
wavelength (Å)	0.979	0.979	0.979
resolution (Å)	50.0–1.95 (2.02–1.95)	93.6–2.17 (2.29–2.17)	50.0–1.95 (2.02–1.95)
no. of observations	579452	277102	489835
no. of unique reflections	88348	63148	139296
$R_{\text{merge}}(I)$	0.061 (0.525)	0.057 (0.583)	0.049 (0.453)
mean I/σ	32.1 (3.4)	16.5 (2.3)	24.2 (2.2)
completeness (%)	99.9 (100.0)	99.8 (98.9)	96.5 (93.0)
multiplicity	6.6 (6.5)	4.4 (4.4)	3.5 (3.3)
no. of protein residues	971	961	2054
no. of atoms	7755	7578	15436
no. of NAD ⁺ atoms	0	62	0
no. of water molecules	245	173	241
no. of PEG atoms	0	0	45
no. of Mg ²⁺ ions	0	0	1
R_{cryst}	0.177 (0.211)	0.173 (0.235)	0.194 (0.228)
R_{free}^b	0.202 (0.240)	0.212 (0.275)	0.235 (0.301)
root-mean-square deviation for bond lengths (Å)	0.007	0.008	0.007
root-mean-square deviation for bond angles (deg)	1.03	1.09	1.01
Ramachandran plot ^c			
favored (%)	98.64	97.99	98.48
outliers (no. of residues)	0	0	0
MolProbity score (percentile)	100	99	100
average B (Å ²)			
protein	27.7	39.6	33.2
NAD ⁺	—	41.5	—
water	26.2	34.4	26.7
PEG	—	—	44.6
Mg ²⁺	—	—	40.5
coordinate error (Å) ^d	0.21	0.26	0.24
PDB entry	4OE6	4OE4	4OE5

^aValues for the outer resolution shell of data are given in parentheses. ^bA 5% test set. A common set was used for refinement of the Put2p structures.

^cThe Ramachandran plots were generated with RAMPAGE via the PDB validation server.⁴⁷ ^dMaximum likelihood-based coordinate error estimate reported by PHENIX.

HsPSCDH were removed by passing the sample through a Ni²⁺-charged HisTrap HP column. The tag-free enzyme was collected in the flow-through, dialyzed into 50 mM Tris, 50 mM NaCl, 0.5 mM EDTA, 0.5 mM THP, and 5% glycerol (pH 8.0), and concentrated to 6 mg/mL for crystallization trials.

Crystal screening revealed a promising crystal form grown in PEG 3350 and MgCl₂. Optimized crystals were grown using a reservoir of 20–25% (w/v) PEG 3350, 0.2 M MgCl₂, and 0.1 M HEPES (pH 7.0–8.0). The crystals were cryoprotected with 25% (w/v) PEG 3350, 0.2 M MgCl₂, 0.1 M HEPES (pH 7.5), and 20% (v/v) PEG 200. The cryoprotected crystals were harvested with nylon loops and plunged into liquid nitrogen. The space group is $P2_1$ with $a = 92.0 \text{ \AA}, b = 121.3 \text{ \AA}, c = 93.4 \text{ \AA}$, and $\beta = 104.2^\circ$. The asymmetric unit contains two dimers and 39% solvent.²¹ This form differs from the hexagonal form of His-tagged HsPSCDH reported previously.¹²

X-ray Diffraction Data Collection, Phasing, and Refinement. Crystals were analyzed at NE-CAT beamlines 24-ID-C and 24-ID-E at the Advanced Photon Source using a Quantum 315 detector (Table 1). The Put2p data set was obtained at beamline 24-ID-C and consisted of 105 frames collected with an oscillation width of 1°, a detector distance of 225 mm, and an exposure time of 1.0 s/frame at 7% transmission. The data were processed to 1.95 Å resolution

using HKL2000.²² Data from Put2p–NAD⁺ crystals were collected at beamline 24-ID-E and processed with XDS.²³ The 2.2 Å resolution data set consisted of 70 frames collected with an oscillation width of 1°, a detector distance of 200 mm, and an exposure time of 1.0 s/frame at 55% transmission. Data from HsPSCDH crystals were collected at beamline 24-ID-C. The data set used for refinement consisted of 180 frames collected with an oscillation width of 1°, a detector distance of 250 mm, and an exposure time of 1.0 s/frame at 4% transmission. The data were processed to 1.95 Å resolution using HKL2000.

The phase problem was solved using molecular replacement as implemented in MOLREP.²⁴ The search model for Put2p was derived from a 1.3 Å resolution structure of mouse PSCDH (PDB entry 3V9J,¹² 43% identical sequence over 543 residues). The search model for HsPSCDH was obtained from a 2.5 Å resolution structure of HsPSCDH (PDB entry 3V9G¹²). The models from molecular replacement were used as the starting points for several rounds of model building with COOT²⁵ and refinement with PHENIX.²⁶ The refined Put2p structure was used as the starting point for refinement of the structure of the Put2p–NAD⁺ complex.

Small-Angle X-ray Scattering of Put2p. In preparation for SAXS studies, wild-type Put2p was purified in a manner similar to that used for crystallization except for the following

modifications. After the first Ni^{2+} affinity step, tobacco etch virus protease was added to the pooled fractions and incubated at 28 °C for 2 h. The protein was then dialyzed overnight against 20 mM HEPES, 100 mM NaCl, and 5% glycerol (pH 8.2). The protein was then injected onto the Ni^{2+} affinity column and eluted at 30 mM imidazole. The fractions were collected, pooled, and dialyzed overnight against 50 mM Tris (pH 7.5), 0.5 mM EDTA, 0.5 mM THP, and 5% glycerol. The protein was further purified using anion exchange (HiTrap Q) and dialyzed into 50 mM Tris, 150 mM NaCl, 0.5 mM EDTA, 0.5 mM THP, and 5% glycerol (pH 8.0). Finally, size exclusion chromatography was performed using a Superdex 200 column that had been equilibrated in dialysis buffer. Protein appearing in the void volume was discarded, while protein that eluted as a single peak that was clearly separated from the void volume was collected. The pooled fractions had a concentration of approximately 3 mg/mL (BCA method). The protein was then concentrated using a Millipore centrifugal unit to 7 mg/mL. The flow-through of the centrifugal unit was reserved as the reference for SAXS. Put2p mutant W193A was prepared similarly, except that the final buffer had a somewhat lower pH and a higher ionic strength [50 mM Tris, 300 mM NaCl, 0.5 mM EDTA, 0.5 mM THP, and 5% glycerol (pH 7.5)].

SAXS experiments were performed at SIBYLS beamline 12.3.1 of the Advanced Light Source through the mail-in program.^{27,28} For each sample, scattering intensities were measured at three nominal protein concentrations. Data were collected for each protein concentration at exposure times of 0.5, 1.0, 3.0, and 6.0 s. The scattering curves collected from the protein samples were corrected for background scattering using intensity data collected from the reference buffer.

The SAXS data were analyzed as follows. Composite scattering curves were generated with PRIMUS²⁹ by scaling and merging the background-corrected low- q region data from the 0.5 s exposure (wild type) or 0.1 s exposure (W193A) with the high- q region data from the 3.0 s exposure (wild type) or 6.0 s exposure (W193A). PRIMUS was also used to perform Guinier analysis. FoXS was used to calculate theoretical scattering profiles from atomic models.³⁰ GNOM was used to calculate pair distribution functions.³¹ The SASTBX server³² was used for shape reconstruction calculations.

Analytical Ultracentrifugation. W193A (His tag removed) was analyzed by sedimentation velocity using a Beckman XL-I analytical ultracentrifuge. Following dialysis to equilibrium against the buffer [50 mM Tris, 300 mM NaCl, 0.5 mM EDTA, 0.5 mM THP, and 5% glycerol (pH 7.5)], the protein solution was diluted with dialysis buffer to yield an absorbance (at 280 nm) of 0.95 in a 1.0 cm path length cuvette. A 400 μL aliquot was loaded into the sample compartment of a double-sector cell, assembled with a 1.2 cm charcoal-Epon centerpiece and quartz windows. A slightly larger volume (430 μL) of dialysis buffer was placed in the reference compartment. The sample cell was placed in the rotor and allowed to equilibrate to 20 °C in the rotor chamber for 2 h under vacuum, prior to beginning the experiment. The sample was then sedimented at 30000 rpm, acquiring data at 4 min intervals, until a total of 170 scans had been collected. The resulting data set was analyzed with SEDFIT version 9.4,³³ using the continuous $c(s)$ and continuous $c(M)$ distribution models, allowing the frictional ratio to float.

Steady-State Kinetics. PSCDH activity was measured with Put2p expressed from pET14b-PUT2, including the N-terminal six-His tag. Put2p activity was followed by monitoring the

formation of NADH at 20 °C as described previously for human PSCDH.¹² The assay buffer contained 50 mM potassium phosphate (pH 7.5) and 25 mM NaCl. The Put2p concentration was 0.4 μM (25.6 $\mu\text{g}/\text{mL}$), and the NAD^+ concentration was held constant at 0.2 mM. Initial velocity data were collected using L-PSC concentrations from 1 to 300 μM . Initial velocity data were fit to the Michaelis–Menten equation to estimate K_m and k_{cat} .

RESULTS

Steady-State Kinetics Measurements. Brandriss and co-workers previously measured Put2p enzymatic activity in cellular and mitochondrial extracts to verify the identity of the enzyme and determine the subcellular location.^{34–36} To the best of our knowledge, the catalytic properties of the purified enzyme have not been studied. We therefore performed steady-state kinetic measurements of recombinant Put2p. Kinetic parameters for Put2p were as follows: $K_m = 104 \pm 4 \mu\text{M}$ L-PSC, and $k_{\text{cat}} = 1.5 \pm 0.3 \text{ s}^{-1}$, with $k_{\text{cat}}/K_m = 14000 \pm 3000 \text{ M}^{-1} \text{ s}^{-1}$. For reference, the kinetic constants for human PSCDH are a K_m of 32 μM L-PSC and a k_{cat} of 10.0 s^{-1} ($k_{\text{cat}}/K_m = 312500 \text{ M}^{-1} \text{ s}^{-1}$).¹²

Protomer Structure of Put2p. The 1.95 Å resolution crystal structure of Put2p was determined (Table 1). Put2p exhibits the expected ALDH fold, which consists of three domains (Figure 2A). The N-terminal half of the polypeptide chain contains a Rossmann fold domain and binds NAD^+

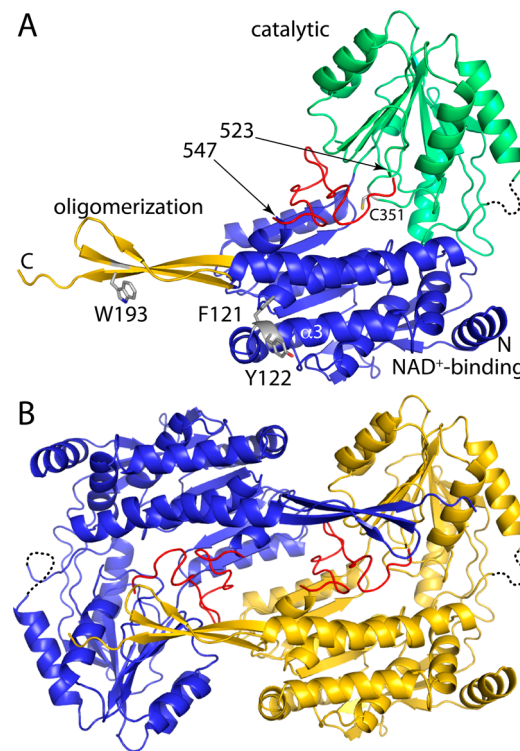


Figure 2. Structure of Put2p. (A) Protomer with the catalytic domain colored green, the NAD^+ -binding domain blue, and the oligomerization domain gold. The red sections represent the aldehyde-binding loop (transplanted from a MmPSCDH structure), which is disordered in Put2p. Selected side chains of the hexamerization hot spot are colored gray (Trp193, Phe121, and Tyr122). (B) Structure of the Put2p dimer in the asymmetric unit. The two protomers are colored blue and gold. Red sections represent the aldehyde-binding loop, which is disordered in Put2p.

(residues 43–181, 200–319, and 536–553). The catalytic domain (residues 320–535) interrupts the NAD⁺-binding domain and exhibits an open α/β fold featuring a twisted seven-stranded β -sheet with all but one strand in parallel. This domain furnishes the essential cysteine nucleophile (Cys351), which is situated at the interface of the NAD⁺-binding and catalytic domains. The third domain is a bipartite β substructure consisting of residues 182–199 and 554–565 that protrudes from the NAD⁺-binding domain. This domain is involved in oligomerization. As with other ALDHs, Put2p forms a dimer in which the oligomerization domain of one protomer engages the catalytic domain of the other protomer (Figure 2B). The asymmetric unit contains one dimer. As described below, three Put2p dimers assemble into a hexamer in solution.

The most conspicuous feature of the Put2p structure is that which is unseen. ALDHs have an ~25-residue peptide that connects the last strand of the catalytic domain to the second piece of the oligomerization domain. This section corresponds to residues 523–547 of Put2p. Electron density for these residues is very weak, implying substantial conformational disorder (Figure 3A). The lack of density for this part of the protein gives the impression of a large void running lengthwise through the middle of the dimer (Figure 3A).

The omission of residues 524–546 from the Put2p model is notable because this region of ALDHs anchors the aldehyde substrate in the active site (Figure 3B). In other PSCDHs (and ALDHs in general), the 25-residue aldehyde-binding loop folds into a two-stranded antiparallel β -sheet that forms the floor of the aldehyde substrate entrance tunnel. In PSCDHs, the beginning of the peptide provides critical hydrogen bonding groups that anchor the backbone of GSA, as well as a conserved Phe that packs against the aliphatic chain of GSA (Figure 3B).^{12,16,18} The observation of disorder in the aldehyde anchor peptide suggests the hypothesis that in solution the anchor peptide samples conformations other than the one that binds the substrate.

Structure of the Put2p–NAD⁺ Complex. The structure of Put2p complexed with NAD⁺ was determined (Table 1). Electron density for the ADP group of NAD⁺ is strong in both protomers (Figure 4). Density for the nicotinamide ribose is strong in one protomer and somewhat weaker in the other. Density for the nicotinamide is diffuse in both protomers, implying disorder, and thus, the nicotinamide was omitted from the final model deposited in the PDB. Disorder of the nicotinamide has been reported for ALDHs.^{12,16,37}

NAD⁺ binds in the expected location, with the adenine ring wedged between valine and proline residues belonging to helices of the Rossmann fold domain (Figure 4). The adenine ribose forms hydrogen bonds with Lys234, and the pyrophosphate interacts with Ser288. The nicotinamide ribose hydrogen bonds with Glu458. These interactions are also observed in the structure of the MmPSCDH–NAD⁺ complex.¹²

Binding of the cofactor is accompanied by side chain rotations (Figure 4). Phe460 rotates around χ_1 by 96° to avoid a steric clash with the nicotinamide ribose. Glu458 rotates by 120°, allowing a hydrogen bond with the nicotinamide ribose. These torsional rotations have not been reported for other PSCDHs.

Structure of Monoclinic HsPSCDH. To further explore the idea that the aldehyde anchor peptide is flexible in solution, the structure of a second eukaryotic PSCDH without a ligand

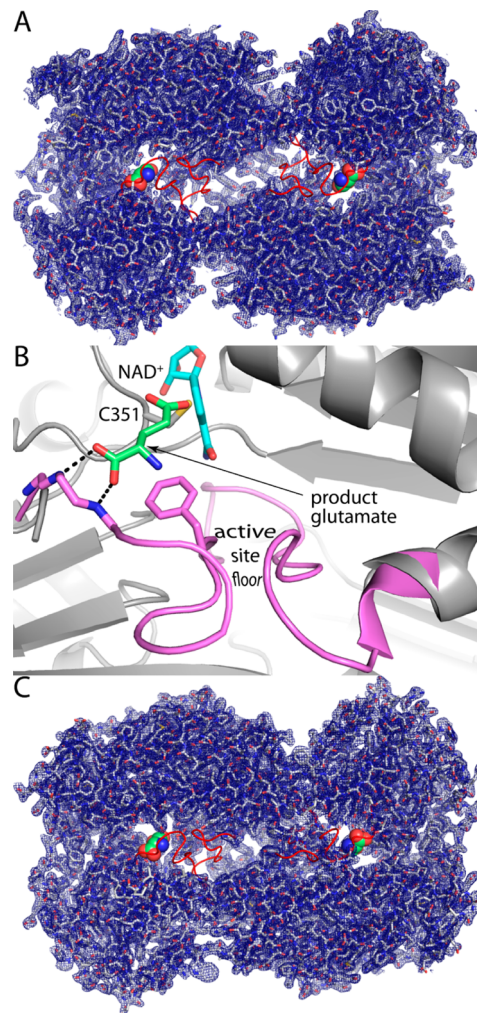


Figure 3. Electron density evidence for disorder in the aldehyde-binding loops of Put2p and HsPSCDH. (A) Put2p dimer with $2F_o - F_c$ electron density (1.0σ). The red sections represent the aldehyde-binding loops transplanted from MmPSCDH. The green spheres represent the product glutamate bound to MmPSCDH (PDB entry 3v9k). (B) Close-up view of the expected conformation of the aldehyde-binding loop in Put2p. Put2p is colored gray. The aldehyde-binding loop (pink), bound glutamate ligand (green), and NAD⁺ of MmPSCDH have been fit onto Put2p to guide the eye. (C) Dimer of monoclinic HsPSCDH with $2F_o - F_c$ electron density (1.0σ). The red sections represent the aldehyde-binding loop of MmPSCDH, which is disordered in the monoclinic crystal form of HsPSCDH. The green spheres represent the product glutamate bound to MmPSCDH.

bound in the aldehyde site was determined. The structure of ligand-free HsPSCDH was determined from a new monoclinic crystal form (Table 1) that was obtained only after cleaving the N-terminal His tag.

As in the Put2p structure, electron density for the aldehyde anchor peptide of monoclinic HsPSCDH (residues 514–535) is very weak (Figure 3C). Electron density for these residues is essentially absent in chains A and D, and the entire loop was omitted. In the other two chains in the asymmetric unit, the binding of Mg²⁺ from the crystallization buffer stabilizes residues 522–535 in a non-native conformation, but the other residues of the loop remain disordered. Thus, the disordered active site is not limited to Put2p.

Oligomeric State and Quaternary Structure of Put2p. The oligomeric state of Put2p in solution was investigated using

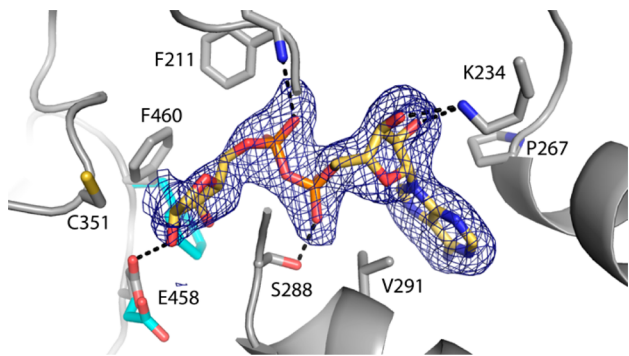


Figure 4. Electron density and interactions for NAD^+ bound to Put2p. The cage represents a simulated annealing σ_A -weighted $F_0 - F_c$ omit map contoured at 3.0σ . The conformations of Glu458 and Phe460 prior to NAD^+ binding are colored cyan.

SAXS (Figure 5). Guinier plots of data from three samples having different protein concentrations yield a radius of

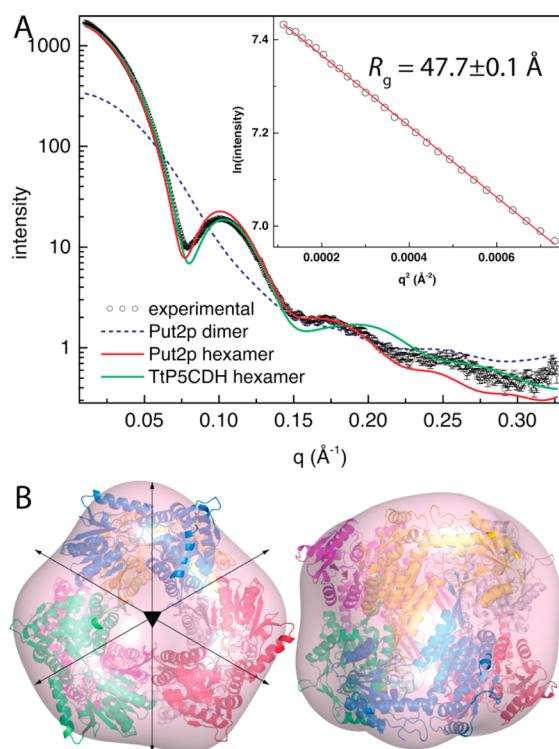


Figure 5. SAXS analyses of Put2p. (A) Experimental and calculated SAXS curves. The inset shows a Guinier plot spanning the qR_g range of $0.508-1.29$. The linear fit of the Guinier plot has an R^2 of 0.9995 . (B) Superposition of the SAXS shape reconstruction envelope and the Put2p hexamer generated from crystallographic symmetry. Two orthogonal views are shown.

gyration (R_g) in the range of $47-48 \text{ \AA}$. Calculations of the pair distribution function suggest a maximal particle dimension of $140-150 \text{ \AA}$ and an R_g of 45 \AA . The R_g of the Put2p dimer in the asymmetric unit (Figure 2B) is only 31.5 \AA , which suggests that a higher-order oligomer is formed in solution. Furthermore, the theoretical SAXS curve calculated from the dimer deviates substantially from the experimental curve (Figure 5A).

The Put2p crystal lattice was inspected to identify a higher-order assembly that is consistent with the SAXS data.

Application of the crystallographic 3-fold rotation to the dimer in the asymmetric unit generates a point group 32 hexamer with an R_g of 43.9 \AA (Figure 5B), which is close to the experimental R_g of 48 \AA . The scattering profile calculated from the Put2p hexamer shows good agreement with the experimental profile (Figure 5A). Slightly better agreement is obtained with the hexamer of TtP5CDH (Figure 5A), which includes the sections that are disordered in Put2p. Consideration of a mixture of hexamers and dimers using minimal ensemble search³⁸ did not improve the fit.

The hexamer oligomeric state was confirmed by estimating the molecular mass from SAXS data using the volume of correlation (V_c) invariant.³⁹ The V_c of Put2p is 1459 \AA^2 , which corresponds to a molecular mass of 363 kDa . This value is within 4% of the expected molecular mass of 376 kDa for a hexamer of the Put2p protein used for SAXS. We concluded that the predominant form of Put2p in solution is the trimer-of-dimers hexamer observed in the crystal lattice.

Finally, shape reconstruction calculations are also consistent with the hexamer. The shape reconstruction was performed with the SASTBX server,³² which makes no explicit assumptions about the molecular mass, the number of residues, or the oligomeric state of the particle under consideration. The envelope is consistent with the crystallographic hexamer (Figure 5B).

Hexamerization Hot Spot of Put2p. We previously identified a hexamerization hot spot in bacterial P5CDHs.¹⁹ The hot spot is located in the interface between two dimers and is formed by $\alpha 3$ of one molecule and the oligomerization domain of another molecule (Figure 6A). In the bacterial P5CDH hexamers, an Arg residue of $\alpha 3$ (e.g., Arg100 of TtP5CDH) is at the center of the hot spot and forms several electrostatic interactions across the dimer–dimer interface (Figure 6C). Mutation of this Arg to Ala in TtP5CDH or DrP5CDH abrogates hexamerization in favor of dimers, showing that it is essential for hexamer formation.

Interestingly, Ala126 of Put2p replaces Arg100 of TtP5CDH, while Trp193 of Put2p replaces Asp166 of TtP5CDH of the oligomerization domain (Figure 6B). Trp193 occupies the space corresponding to the Arg100 side chain of TtP5CDH. The indole of Trp193 fits into a hole formed by several residues of $\alpha 3$ (Phe121, Tyr122, Ser125, Ala126, and Leu129) as well as Val174 of $\alpha 5$ (Figure 6B). We therefore hypothesized that Trp193 is the center of the hexamerization hot spot of Put2p, analogous to the essential Arg of TtP5CDH and DrP5CDH. This idea was tested by creating Put2p variant W193A.

The oligomeric state of W193A was determined using sedimentation velocity. Figure 7A displays a subset of the velocity profiles, with the corresponding least-squares fits. Analysis of the entire data set with SEDFIT yielded a symmetric sedimentation coefficient distribution centered at 4.65 S (Figure 7B). The corresponding molecular mass distribution is centered at 121 kDa (Figure 7C), which is within 3% of the theoretical M of the W193A dimer (125 kDa). Thus, mutation of Trp193 to Ala appears to have disrupted the hexamer, as intended.

W193A was also analyzed using SAXS (Figure 8). Guinier plots of data from three samples having different protein concentrations yield an R_g in the range of $34.5-34.7 \text{ \AA}$. Calculations of the pair distribution function suggest a maximal particle dimension of $110-115 \text{ \AA}$ and an R_g of 34.7 \AA . As stated above, the R_g of the Put2p dimer in the asymmetric unit is 31.5 \AA , whereas that of the hexamer is 44 \AA . Thus, the R_g of W193A

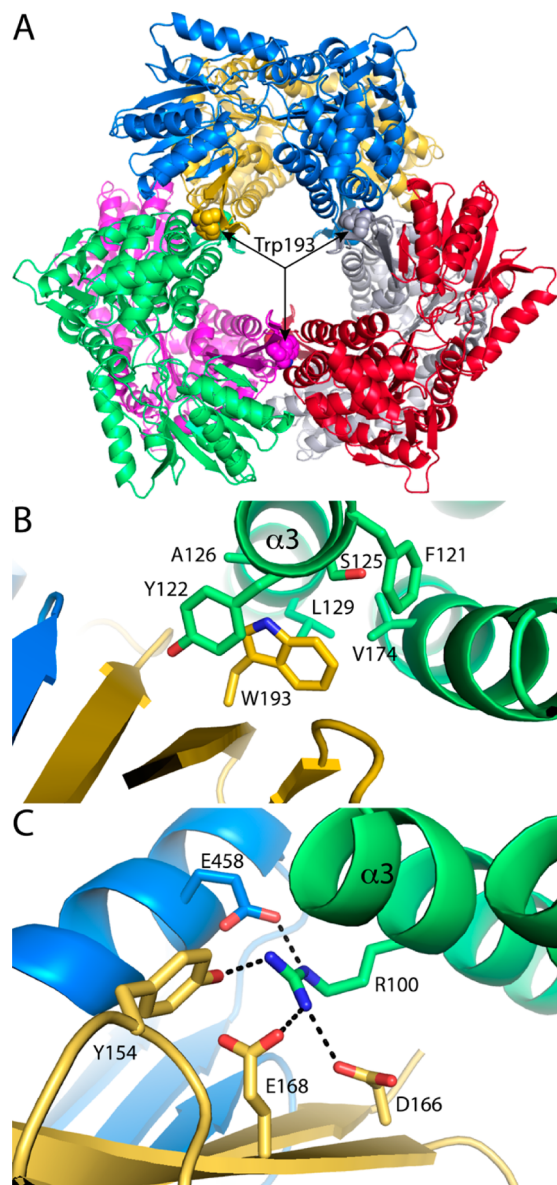


Figure 6. Hexamerization hot spots of Put2p and TtPSCDH. (A) Put2p hexamer viewed down the 3-fold axis, showing the location of the hot spot centered on Trp193 (shown as spheres). The six chains have different colors. (B) Close-up view of the environment around Trp193 of Put2p. The chains are colored as in panel A. (C) Hot spot of TtPSCDH, which is centered on Arg100 of α_3 . The chains are colored as in panel A.

is consistent with a dimer in solution. The theoretical SAXS curve calculated from the Put2p dimer agrees well with the experimental one, while the curve derived from the hexamer curve shows significant deviation (Figure 8A). Furthermore, the envelope from shape reconstruction calculations, performed with the SASTBX server, is consistent with the crystallographic dimer (Figure 8B). Thus, the SAXS data are also consistent with W193A being primarily dimeric in solution.

DISCUSSION

The disordered aldehyde anchor loop is the major result from the Put2p and HsPSCDH crystal structures reported here. It is tempting to speculate that these structures represent the resting enzyme conformation, implying that aldehyde binding stabilizes

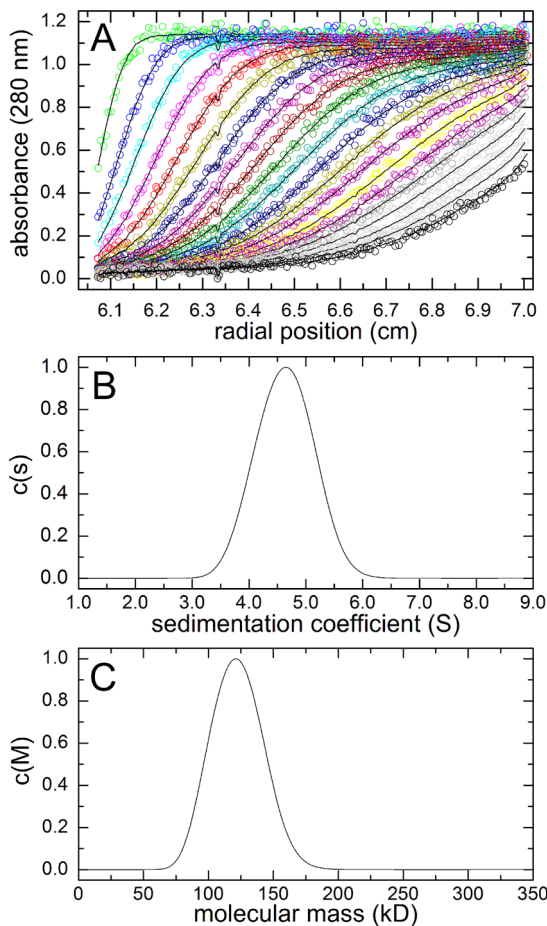


Figure 7. Sedimentation velocity analysis of W193A. (A) Selected velocity profiles (circles) and optimal least-squares fits. (B) Sedimentation coefficient distribution. (C) Molecular mass distribution.

the active site. This interpretation is supported by the fact that all other structures of eukaryotic PSCDHs (human and mouse) have ligands bound in the aldehyde site, including sulfate ion from the crystallization buffer (PDB entries 3V9J and 3V9H),¹² the product glutamate (PDB entry 3V9K),¹² and proline (PDB entry 4E3X),⁴⁰ which is a competitive inhibitor with respect to GSA.¹ Although a ligand was not modeled in two other structures (PDB entries 3V9L and 3V9G), electron density consistent with an active site ligand, probably sulfate ion, is nevertheless evident. Thus, none of the previously determined structures of eukaryotic PSCDHs are truly representative of the aldehyde-free conformation. Bacterial PSCDH structures, however, provide a counterargument; a few bacterial PSCDHs have an ordered active site in the absence of a ligand in the aldehyde site (e.g., PDB entries 2EHQ, 2BHP, and 3RJL). Nevertheless, the observation that the aldehyde anchor peptide is disordered in two different PSCDHs that were crystallized in unrelated lattices suggests that the disorder may be functionally relevant, at least for eukaryotic PSCDHs. At the very least, the structures provide evidence that the aldehyde-binding loop is inherently flexible, possibly sampling active and inactive conformations in the absence of the substrate. In this view, Put2p would be an example of substrate recognition by conformational selection.⁴¹ These results add a new dimension to our understanding of ALDH substrate specificity.⁴²

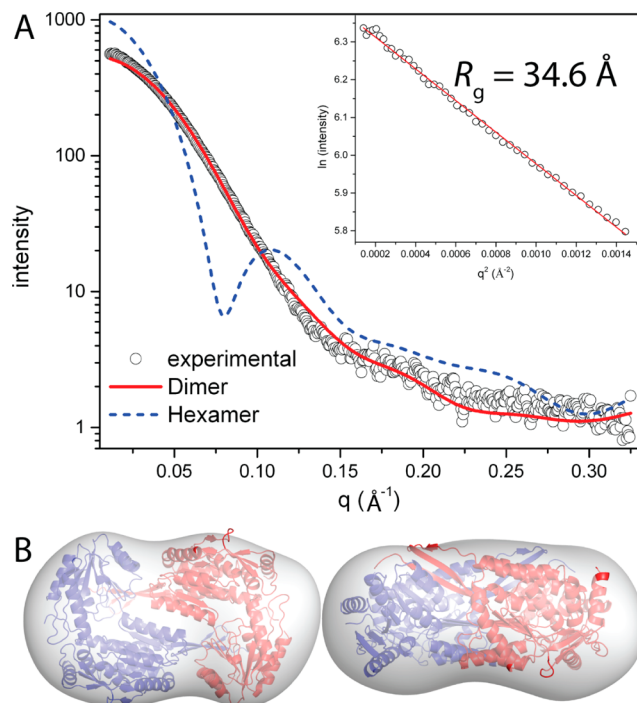


Figure 8. SAXS analysis of W193A. (A) Experimental and calculated SAXS curves. The inset shows a Guinier plot spanning the qR_g range of 0.346–1.34. The linear fit of the Guinier plot has an R^2 of 0.997. (B) Superposition of the SAXS shape reconstruction envelope and the Put2p dimer from the asymmetric unit. Two orthogonal views are shown.

Disorder in enzyme active sites on the scale described here has precedent, and retinal dehydrogenase II is the most germane example. Also a member of the ALDH superfamily, retinal dehydrogenase II catalyzes the oxidation of retinal to retinoic acid and is thus involved in retinoic acid signaling. As in Put2p, the aldehyde-binding loop is disordered in the crystal structure of retinal dehydrogenase II (PDB entry 1BI9). It has been proposed that the disordered loop plays a role in discriminating retinal from smaller potential substrates.^{43,44}

The discovery that Put2p is hexameric is unexpected. Put2p and HsPSCDH are eukaryotic PSCDHs that have 42% identical amino acid sequences, yet Put2p is hexameric and HsPSCDH dimeric.¹² The trimer-of-dimers hexamer described here for Put2p is also formed by TtPSCDH and DrPSCDH,¹⁹ although Put2p is only 30% identical to these bacterial PSCDHs. Curiously, other bacterial PSCDHs, such as those from *Bacillus* species, are dimeric.¹⁹ Thus, global sequence identity and domain of life are poor predictors of the oligomeric states of PSCDHs. Instead, we suggest that the hot spot theory of protein–protein association provides a better explanation.^{45,46}

The Put2p structure revealed Trp193 as a potential hot spot residue. Trp193 is located in the same region as the bacterial hexamerization hot spot, where it forms nonpolar, knob-in-hole interactions across the dimer–dimer interface (Figure 6B). Furthermore, Trp, along with Tyr and Arg, is often found in protein–protein interface hot spots.⁴⁵ Mutation of Trp193 to Ala abrogates hexamer formation, suggesting that these nonpolar interactions (Figure 6B) substitute for the electrostatic interactions that stabilize the bacterial PSCDH hexamers (Figure 6C). Thus, the ALDH4A1 hexamerization hot spot appears to be a unique region of three-dimensional structural space that must be occupied by residues capable of forming

attractive intermolecular forces for hexamerization to occur. Interestingly, the precise nature of these forces appears to be less important than their location.

Finally, the hot spot theory provides a satisfactory explanation for why some PSCDHs are dimeric. A theoretical hexamer built from HsPSCDH dimers has vacant space in the hot spot region instead of the tight knob-in-hole interaction observed in Put2p. The result reflects the fact that the mammalian enzymes have the short residue Thr in place of Trp193. Also, hexamers built from the *Bacillus* PSCDH dimers show steric clashes of long side chains across the dimer–dimer interface. Thus, the dimeric enzymes do not have an appropriate constellation of residues for building a functional hexamerization hot spot.

ASSOCIATED CONTENT

Accession Codes

Atomic coordinates and structure factors have been deposited in the Protein Data Bank as entries 4OE6 (Put2p), 4OE4 (Put2p–NAD⁺ complex), and 4OES (HsPSCDH).

AUTHOR INFORMATION

Corresponding Author

*Department of Biochemistry, University of Missouri—Columbia, Columbia, MO 65211. E-mail: tannerjj@missouri.edu. Phone: (573) 884-1280. Fax: (573) 882-2754.

Funding

Research reported in this publication was supported by the National Institute of General Medical Sciences of the National Institutes of Health via Grant GM065546.

Notes

The authors declare no competing financial interest.

ACKNOWLEDGMENTS

We thank Kevin Dyer of the SIBYLS beamline of the Advanced Light Source for collecting the SAXS data, Dr. Marjorie Brandriss of the Rutgers New Jersey Medical School for providing the PUT2 clone, and Dr. Jonathan Schuermann of the Northeastern Collaborative Access Team at the Advanced Photon Source for help with diffraction data collection and processing. Part of this work is based upon research conducted at the Advanced Photon Source on the Northeastern Collaborative Access Team beamlines, which are supported by a grant from the National Institute of General Medical Sciences (P41 GM103403) from the National Institutes of Health. Use of the Advanced Photon Source, an Office of Science User Facility operated for the U.S. Department of Energy (DOE) Office of Science by Argonne National Laboratory, was supported by the DOE under Contract DE-AC02-06CH11357. Part of this work was conducted at the Advanced Light Source (ALS), a national user facility operated by Lawrence Berkeley National Laboratory on behalf of the Department of Energy, Office of Basic Energy Sciences, through the Integrated Diffraction Analysis Technologies (IDAT) program, supported by DOE Office of Biological and Environmental Research. Additional support comes from the National Institutes of Health project MINOS (R01GM105404).

ABBREVIATIONS

PRODH, proline dehydrogenase; PSC, Δ^1 -pyrroline-5-carboxylate; GSA, γ -glutamate semialdehyde; PSCDH, Δ^1 -pyrroline-5-

carboxylate dehydrogenase; PutA, proline utilization A; Put2p, *S. cerevisiae* Δ^1 -pyrroline-5-carboxylate dehydrogenase; PUT2, gene encoding *S. cerevisiae* Δ^1 -pyrroline-5-carboxylate dehydrogenase; Put1p, *S. cerevisiae* proline dehydrogenase; HsP5CDH, human Δ^1 -pyrroline-5-carboxylate dehydrogenase; MmP5CDH, mouse Δ^1 -pyrroline-5-carboxylate dehydrogenase; TtP5CDH, *T. thermophilus* Δ^1 -pyrroline-5-carboxylate dehydrogenase; DrP5CDH, *D. radiodurans* Δ^1 -pyrroline-5-carboxylate dehydrogenase; SAXS, small-angle X-ray scattering; THP, tris(hydroxymethyl)phosphate.

■ REFERENCES

- (1) Wanduragala, S., Sanyal, N., Liang, X., and Becker, D. F. (2010) Purification and characterization of Put1p from *Saccharomyces cerevisiae*. *Arch. Biochem. Biophys.* 498, 136–142.
- (2) Vasilicou, V., and Nebert, D. W. (2005) Analysis and update of the human aldehyde dehydrogenase (ALDH) gene family. *Hum. Genomics* 2, 138–143.
- (3) Liang, X., Zhang, L., Natarajan, S. K., and Becker, D. F. (2013) Proline Mechanisms of Stress Survival. *Antioxid. Redox Signaling* 19, 998–1011.
- (4) Morita, Y., Nakamori, S., and Takagi, H. (2002) Effect of proline and arginine metabolism on freezing stress of *Saccharomyces cerevisiae*. *J. Biosci. Bioeng.* 94, 390–394.
- (5) Nishimura, A., Nasuno, R., and Takagi, H. (2012) The proline metabolism intermediate Δ^1 -pyrroline-5-carboxylate directly inhibits the mitochondrial respiration in budding yeast. *FEBS Lett.* 586, 2411–2416.
- (6) Nomura, M., and Takagi, H. (2004) Role of the yeast acetyltransferase Mpr1 in oxidative stress: Regulation of oxygen reactive species caused by a toxic proline catabolism intermediate. *Proc. Natl. Acad. Sci. U.S.A.* 101, 12616–12621.
- (7) Magasanik, B., and Kaiser, C. A. (2002) Nitrogen regulation in *Saccharomyces cerevisiae*. *Gene* 290, 1–18.
- (8) Nasuno, R., Hirano, Y., Itoh, T., Hakoshima, T., Hibi, T., and Takagi, H. (2013) Structural and functional analysis of the yeast N-acetyltransferase Mpr1 involved in oxidative stress tolerance via proline metabolism. *Proc. Natl. Acad. Sci. U.S.A.* 110, 11821–11826.
- (9) Forte-McRobbie, C., and Pietruszko, R. (1989) Human glutamic γ -semialdehyde dehydrogenase. Kinetic mechanism. *Biochem. J.* 261, 935–943.
- (10) Forte-McRobbie, C. M., and Pietruszko, R. (1986) Purification and characterization of human liver “high Km” aldehyde dehydrogenase and its identification as glutamic γ -semialdehyde dehydrogenase. *J. Biol. Chem.* 261, 2154–2163.
- (11) Small, W. C., and Jones, M. E. (1990) Pyrroline 5-carboxylate dehydrogenase of the mitochondrial matrix of rat liver. Purification, physical and kinetic characteristics. *J. Biol. Chem.* 265, 18668–18672.
- (12) Srivastava, D., Singh, R. K., Moxley, M. A., Henzl, M. T., Becker, D. F., and Tanner, J. J. (2012) The Three-Dimensional Structural Basis of Type II Hyperprolinemia. *J. Mol. Biol.* 420, 176–189.
- (13) Valle, D., Goodman, S. I., Applegarth, D. A., Shih, V. E., and Phang, J. M. (1976) Type II hyperprolinemia. Δ^1 -Pyrroline-5-carboxylic acid dehydrogenase deficiency in cultured skin fibroblasts and circulating lymphocytes. *J. Clin. Invest.* 58, 598–603.
- (14) Geraghty, M. T., Vaughn, D., Nicholson, A. J., Lin, W. W., Jimenez-Sanchez, G., Obie, C., Flynn, M. P., Valle, D., and Hu, C. A. (1998) Mutations in the Δ^1 -pyrroline 5-carboxylate dehydrogenase gene cause type II hyperprolinemia. *Hum. Mol. Genet.* 7, 1411–1415.
- (15) Phang, J. M., Hu, C. A., and Valle, D. (2001) Disorders of proline and hydroxyproline metabolism. In *Metabolic and molecular basis of inherited disease* (Scriver, C. R., Beaudet, A. L., Sly, W. S., and Valle, D., Eds.) pp 1821–1838, McGraw-Hill, New York.
- (16) Inagaki, E., Ohshima, N., Takahashi, H., Kuroishi, C., Yokoyama, S., and Tahirov, T. H. (2006) Crystal structure of *Thermus thermophilus* Δ^1 -pyrroline-5-carboxylate dehydrogenase. *J. Mol. Biol.* 362, 490–501.
- (17) Inagaki, E., Ohshima, N., Sakamoto, K., Babayeva, N. D., Kato, H., Yokoyama, S., and Tahirov, T. H. (2007) New insights into the binding mode of coenzymes: Structure of *Thermus thermophilus* Δ^1 -pyrroline-5-carboxylate dehydrogenase complexed with NADP⁺. *Acta Crystallogr. F* 63, 462–465.
- (18) Pemberton, T. A., and Tanner, J. J. (2013) Structural basis of substrate selectivity of Δ^1 -pyrroline-5-carboxylate dehydrogenase (ALDH4A1): Semialdehyde chain length. *Arch. Biochem. Biophys.* 538, 34–40.
- (19) Luo, M., Singh, R. K., and Tanner, J. J. (2013) Structural determinants of oligomerization of Δ^1 -pyrroline-5-carboxylate dehydrogenase: Identification of a hexamerization hot spot. *J. Mol. Biol.* 425, 3106–3120.
- (20) Martin, O., Brandriss, M. C., Schneider, G., and Bakalinsky, A. T. (2003) Improved anaerobic use of arginine by *Saccharomyces cerevisiae*. *Appl. Environ. Microbiol.* 69, 1623–1628.
- (21) Matthews, B. W. (1968) Solvent content of protein crystals. *J. Mol. Biol.* 33, 491–497.
- (22) Otwinowski, Z., and Minor, W. (1997) Processing of X-ray diffraction data collected in oscillation mode. *Methods Enzymol.* 276, 307–326.
- (23) Kabsch, W. (2010) XDS. *Acta Crystallogr. D* 66, 125–132.
- (24) Vagin, A., and Teplyakov, A. (1997) MOLREP: An automated program for molecular replacement. *J. Appl. Crystallogr.* 30, 1022–1025.
- (25) Emsley, P., and Cowtan, K. (2004) Coot: Model-building tools for molecular graphics. *Acta Crystallogr. D* 60, 2126–2132.
- (26) Adams, P. D., Afonine, P. V., Bunkoczi, G., Chen, V. B., Davis, I. W., Echols, N., Headd, J. J., Hung, L. W., Kapral, G. J., Grosjean-Kunstleve, R. W., McCoy, A. J., Moriarty, N. W., Oeffner, R., Read, R. J., Richardson, D. C., Richardson, J. S., Terwilliger, T. C., and Zwart, P. H. (2010) PHENIX: A comprehensive Python-based system for macromolecular structure solution. *Acta Crystallogr. D* 66, 213–221.
- (27) Hura, G. L., Menon, A. L., Hammel, M., Rambo, R. P., Poole, F. L., II, Tsutakawa, S. E., Jenney, F. E., Jr., Classen, S., Frankel, K. A., Hopkins, R. C., Yang, S. J., Scott, J. W., Dillard, B. D., Adams, M. W., and Tainer, J. A. (2009) Robust, high-throughput solution structural analyses by small angle X-ray scattering (SAXS). *Nat. Methods* 6, 606–612.
- (28) Classen, S., Hura, G. L., Holton, J. M., Rambo, R. P., Rodic, I., McGuire, P. J., Dyer, K., Hammel, M., Meigs, G., Frankel, K. A., and Tainer, J. A. (2013) Implementation and performance of SIBYLS: A dual endstation small-angle X-ray scattering and macromolecular crystallography beamline at the Advanced Light Source. *J. Appl. Crystallogr.* 46, 1–13.
- (29) Konarev, P. V., Volkov, V. V., Sokolova, A. V., Koch, M. H. J., and Svergun, D. I. (2003) PRIMUS: A Windows PC-based system for small-angle scattering data analysis. *J. Appl. Crystallogr.* 36, 1277–1282.
- (30) Schneidman-Duhovny, D., Hammel, M., and Sali, A. (2010) FoXS: A web server for rapid computation and fitting of SAXS profiles. *Nucleic Acids Res.* 38, W540–W544.
- (31) Svergun, D. (1992) Determination of the regularization parameter in indirect-transform methods using perceptual criteria. *J. Appl. Crystallogr.* 25, 495–503.
- (32) Liu, H., Hexemer, A., and Zwart, P. H. (2012) The Small Angle Scattering ToolBox (SASTBX): An open-source software for biomolecular small-angle scattering. *J. Appl. Crystallogr.* 45, 587–593.
- (33) Schuck, P. (2000) Size-distribution analysis of macromolecules by sedimentation velocity ultracentrifugation and Lamm equation modeling. *Biophys. J.* 78, 1606–1619.
- (34) Brandriss, M. C., and Krzywicki, K. A. (1986) Amino-terminal fragments of Δ^1 -pyrroline-5-carboxylate dehydrogenase direct β -galactosidase to the mitochondrial matrix in *Saccharomyces cerevisiae*. *Mol. Cell. Biol.* 6, 3502–3512.
- (35) Brandriss, M. C., and Magasanik, B. (1979) Genetics and physiology of proline utilization in *Saccharomyces cerevisiae*: Enzyme induction by proline. *J. Bacteriol.* 140, 498–503.

- (36) Brandriss, M. C. (1983) Proline utilization in *Saccharomyces cerevisiae*: Analysis of the cloned PUT2 gene. *Mol. Cell. Biol.* 3, 1846–1856.
- (37) Perez-Miller, S. J., and Hurley, T. D. (2003) Coenzyme isomerization is integral to catalysis in aldehyde dehydrogenase. *Biochemistry* 42, 7100–7109.
- (38) Pelikan, M., Hura, G. L., and Hammel, M. (2009) Structure and flexibility within proteins as identified through small angle X-ray scattering. *Gen. Physiol. Biophys.* 28, 174–189.
- (39) Rambo, R. P., and Tainer, J. A. (2013) Accurate assessment of mass, models and resolution by small-angle scattering. *Nature* 496, 477–481.
- (40) Pemberton, T. A., Still, B. R., Christensen, E. M., Singh, H., Srivastava, D., and Tanner, J. J. (2012) Proline: Mother Nature's cryoprotectant applied to protein crystallography. *Acta Crystallogr. D68*, 1010–1018.
- (41) Vogt, A. D., and Di Cera, E. (2013) Conformational selection is a dominant mechanism of ligand binding. *Biochemistry* 52, 5723–5729.
- (42) Riveros-Rosas, H., Gonzalez-Segura, L., Julian-Sanchez, A., Diaz-Sanchez, A. G., and Munoz-Clares, R. A. (2013) Structural determinants of substrate specificity in aldehyde dehydrogenases. *Chem.-Biol. Interact.* 202, 51–61.
- (43) Lamb, A. L., and Newcomer, M. E. (1999) The structure of retinal dehydrogenase type II at 2.7 Å resolution: Implications for retinal specificity. *Biochemistry* 38, 6003–6011.
- (44) Bordelon, T., Montegudo, S. K., Pakhomova, S., Oldham, M. L., and Newcomer, M. E. (2004) A disorder to order transition accompanies catalysis in retinaldehyde dehydrogenase type II. *J. Biol. Chem.* 279, 43085–43091.
- (45) Bogan, A. A., and Thorn, K. S. (1998) Anatomy of hot spots in protein interfaces. *J. Mol. Biol.* 280, 1–9.
- (46) Moreira, I. S., Fernandes, P. A., and Ramos, M. J. (2007) Hot spots: A review of the protein-protein interface determinant amino-acid residues. *Proteins* 68, 803–812.
- (47) Lovell, S. C., Davis, I. W., Arendall, W. B., III, de Bakker, P. I., Word, J. M., Prisant, M. G., Richardson, J. S., and Richardson, D. C. (2003) Structure validation by $C\alpha$ geometry: ϕ , ψ and $C\beta$ deviation. *Proteins* 50, 437–450.